Inorganic Chemistry

Article

pubs.acs.org/IC

Five-Coordinate $[Pt^{II}(bipyridine)_2(phosphine)]^{n+}$ Complexes: Long-Lived Intermediates in Ligand Substitution Reactions of $[Pt(bipyridine)_2]^{2+}$ with Phosphine Ligands

Warrick K. C. Lo,[†] Germán Cavigliasso,[‡] Robert Stranger,[‡] James D. Crowley,*[,†] and Allan G. Blackman*[,†,§]

[†]Department of Chemistry, University of Otago, P.O. Box 56, Dunedin 9054, New Zealand

[‡]Research School of Chemistry, Australian National University, Canberra, ACT 0200, Australia

[§]School of Applied Sciences, Auckland University of Technology, Private Bag 92006, Auckland 1142, New Zealand

Supporting Information

ABSTRACT: The reaction of $[Pt(N{-}N)_2]^{2+}$ [N−N = 2,2′-bipyridine (bpy) or 4,4′-dimethyl-2,2′-bipyridine (4,4′-Me_2bpy)] with phosphine ligands [PPh_3 or $PPh(PhSO_3)_2^{2-}$] in aqueous or methanolic solutions was studied by multinuclear (^1H, ^{13}C, ^{31}P, and ^{195}Pt) NMR spectroscopy, X-ray crystallography, UV−visible spectroscopy, and high-resolution mass spectrometry. NMR spectra of solutions containing equimolar amounts of $[Pt(N{-}N)_2]^{2+}$ and phosphine ligand give evidence for rapid formation of long-lived, 5-coordinate $[Pt^{II}(N{-}N)_2(phosphine)]^{n+}$ complexes. In the presence of excess phosphine ligand, these intermediates undergo much slower entry of a second phosphine ligand and loss of a bpy ligand to give $[Pt^{II}(N{-}N)(phosphine)_2]^{n+}$ as the final product. The coordination of a phosphine ligand to the Pt(II) ion in the intermediate $[Pt(N{-}N)_2(phosphine)]^{n+}$ complexes is supported by the observation of $^{31}P{-}^{195}Pt$ coupling in the ^{31}P NMR spectra. The 5-coordinate nature of $[Pt(bpy)_2\{PPh(PhSO_3)_2\}]$ is confirmed by X-ray crystallography. X-ray crystal structural analysis shows that the Pt(II) ion in $[Pt(bpy)_2\{PPh(PhSO_3)_2\}]\cdot 5.5H_2O$ displays a distorted square pyramidal geometry, with one bpy ligand bound asymmetrically. These results provide strong support for the widely accepted associative ligand substitution mechanism for square planar Pt(II) complexes. X-ray structural characterization of the distorted square planar complex $[Pt(bpy)(PPh_3)_2](ClO_4)_2$ confirms this as the final product of the reaction of $[Pt(bpy)_2]^{2+}$ with PPh_3 in CD_3OD. The results of density functional calculations on $[Pt(bpy)_2]^{2+}$, $[Pt(bpy)_2(phosphine)]^{n+}$, and $[Pt(bpy)(phosphine)_2]^{n+}$ indicate that the bonding energy follows the trend of $[Pt(bpy)(phosphine)_2]^{n+} > [Pt(bpy)_2(phosphine)]^{n+} > [Pt(bpy)_2]^{2+}$ for stability and that the formation reactions of $[Pt(bpy)_2(phosphine)]^{n+}$ from $[Pt(bpy)_2]^{2+}$ and $[Pt(bpy)(phosphine)_2]^{n+}$ from $[Pt(bpy)_2(phosphine)]^{n+}$ are energetically favorable. These calculations suggest that the driving force for the formation of $[Pt(bpy)(phosphine)_2]^{n+}$ from $[Pt(bpy)_2]^{2+}$ is the formation of a more energetically favorable product.

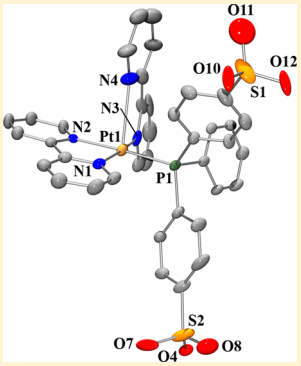

INTRODUCTION

The unusually facile reactivity of the $[Pt(bpy)_2]^{2+}$ (bpy = 2,2′-bipyridine) ion toward a variety of nucleophiles has been a topic of interest ever since Gillard and Lyons first reported some 40 years ago that dissolution of $[Pt(bpy)_2]^{2+}$ in alkaline aqueous solution gave UV−visible spectral changes that were reversible on addition of acid.[1] The considerable amount of data that has been collected by numerous groups since this time has variously been used as evidence that these spectral changes arise from either OH^- attack at the coordinated bpy ligand to give a covalent hydrate or from OH^- coordination to the Pt(II) ion to give a 5-coordinate complex (Scheme 1).[1−13] However, despite the use of numerous physical techniques, it appears that, in the absence of crystal structural data, a definitive experiment to distinguish unequivocally between the two possibilities (see **1** and **2** of Scheme 1) has yet to be devised.[14] It has also been proposed that $[Pt(bpy)_2]^{2+}$ reacts with a variety of anions other than OH^- and heterocyclic nitrogenous bases to give 5-coordinate $[Pt^{II}(bpy)_2(L)]^{n+}$ (L = monodentate ligand) complexes;[13,15,16] evidence for this has come from NMR, UV−vis spectroscopy, and mass spectrometry, but again, a lack of X-ray crystal structural data renders these data open to other interpretations.

The closely related complex cation $[Pt(phen)_2]^{2+}$ reacts with CN^- in aqueous solutions to give the 5-coordinate $[Pt(phen)_2(CN)]^+$ ion, as shown by Wernberg and Hazell, who reported the X-ray crystal structure of $[Pt(phen)_2(CN)](NO_3)\cdot H_2O$ in 1980.[17] The observation of ^{195}Pt satellites in the ^{13}C NMR spectrum of this complex showed that the 5-coordinate structure persists in solution.

Of all the ligands studied in these types of reactions, those having P donor atoms have been surprisingly absent, given that ^{31}P NMR should be potentially useful in the characterization of products formed from such ligands. Herein we report the results of studies of the reactions of $[Pt(N{-}N)_2]^{2+}$ [N−N =

Received: December 19, 2013
Published: March 21, 2014

   dx.doi.org/10.1021/ic403089j | Inorg. Chem. 2014, 53, 3595−3605

Scheme 1. Proposed Products from the Reaction of $[Pt(bpy)_2]^{2+}$ and OH^- in Aqueous Solution[a]

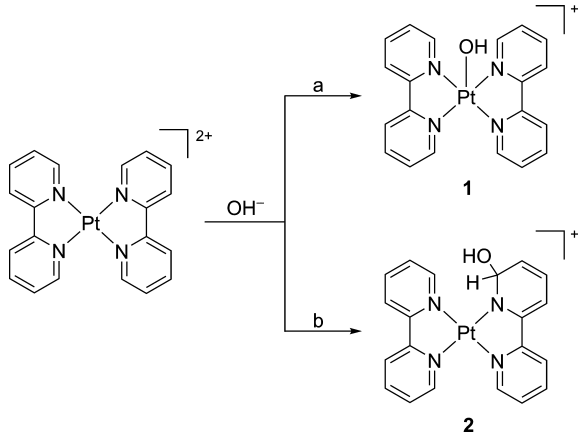

[a]Pathway **a** gives the 5-coordinate complex **1**, $[Pt(bpy)_2(OH)]^+$, through coordination of OH^- to the Pt(II) ion, while compound **2**, a covalent hydrate, is formed via pathway **b** as a result of nucleophilic attack by OH^- at the bpy ligand.

2,2′-bipyridine (bpy) or 4,4′-dimethyl-2,2′-bipyridine (4,4′-Me_2bpy)] toward the phosphine ligands triphenylphosphine (PPh_3) and its water-soluble derivative bis(*p*-sulfonatophenyl)-phenylphosphine $[PPh(PhSO_3)_2^{2-}]$ (Figure 1) in both aqueous and methanolic solutions.

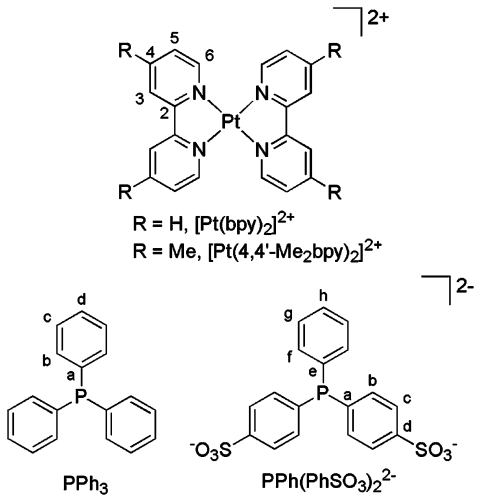

Figure 1. $[Pt(N{-}N)_2]^{2+}$ complexes and phosphine ligands used in this study.

We detail the synthesis of the 5-coordinate Pt(II) complexes $[Pt(N{-}N)_2(L)](NO_3)_n$ (N−N = bpy, 4,4′-Me_2bpy; L = $PPh(PhSO_3)_2^{2-}$, *n* = 0: L = PPh_3, *n* = 2: Scheme 2) and the X-ray crystal structures of both $[Pt(bpy)_2\{PPh(PhSO_3)_2\}]\cdot 5.5H_2O$, the first example of a crystallographically characterized monomeric 5-coordinate $[Pt^{II}(bpy)_2(L)]^{n+}$ complex, and $[Pt(bpy)(PPh_3)_2](ClO_4)_2\cdot 0.5(C_6H_{14}O)$, the product deriving from the 5-coordinate $[Pt(bpy)_2(PPh_3)]^{2+}$ intermediate. We present multinuclear (^1H, ^{13}C, ^{31}P, ^{195}Pt) NMR and mass spectral data from solution studies of the $[Pt(N{-}N)_2(L)](NO_3)_n$ complexes and show that these complexes are fluxional 5-coordinate species in solution at room temperature. Finally, we report the results of density functional theory (DFT) calculations on $[Pt(bpy)_2]^{2+}$, $[Pt^{II}(bpy)_2(L)]^{n+}$, and $[Pt^{II}(bpy)(L)_2]^{n+}$ complexes.

Scheme 2. Synthesis of the 5-Coordinate $[Pt(N{-}N)_2(L)](NO_3)_n$ Complexes[a]

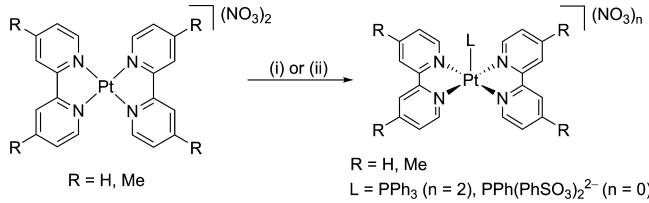

[a]Reaction conditions: (i) 1 equiv of $K_2PPh(PhSO_3)_2\cdot 2H_2O$, H_2O solvent and (ii) 1 equiv of PPh_3, CH_3OH solvent.

RESULTS AND DISCUSSION

Synthesis and Characterization of $[Pt(N{-}N)_2\{PPh(PhSO_3)_2\}]$ Complexes. Addition of 1 equiv of the water-soluble phosphine ligand $K_2PPh(PhSO_3)_2\cdot 2H_2O$ to a pale yellow aqueous solution of $[Pt(bpy)_2](NO_3)_2\cdot H_2O$ at room temperature results in a rapid intensification of the yellow color. The UV−vis absorption spectrum of an aqueous solution of $[Pt(bpy)_2](NO_3)_2\cdot H_2O$ shows two maxima in the UV region, at 245 and 323 nm. On addition of increasing amounts of $K_2PPh(PhSO_3)_2\cdot 2H_2O$ the intensity of the former decreases, while that of the latter increases; three isosbestic points are also observed (Supporting Information, Figure S35). These absorbance changes are similar to those observed in the reaction of $[Pt(bpy)_2](NO_3)_2\cdot H_2O$ and OH^- in water,[1] suggesting that they arise from analogous processes in both complexes.

^1H, ^{13}C, ^{31}P, and ^{195}Pt NMR data were collected from an equimolar mixture of $K_2PPh(PhSO_3)_2\cdot 2H_2O$ and $[Pt(bpy)_2](NO_3)_2\cdot H_2O$ in D_2O, while various two-dimensional NMR experiments were also carried out. Both the ^1H and ^{13}C NMR spectra of the solution gave evidence for chemical reaction, with noticeable changes in the chemical shifts of the signals due to the bpy ligands and the $PPh(PhSO_3)_2^{2-}$ ligand (Supporting Information, Figures S6, S7). The ^{31}P and ^{195}Pt NMR spectra of the solution exhibited signals having chemical shifts significantly different from those of the starting materials (^{31}P NMR, $K_2PPh(PhSO_3)_2\cdot 2H_2O$, −6.79 ppm, singlet; product, 11.13 ppm, singlet with ^{195}Pt and ^{13}C satellites: ^{195}Pt NMR, $[Pt(bpy)_2](NO_3)_2\cdot H_2O$, −2270 ppm, singlet; product, −3176 ppm, doublet). In addition, $^{31}P{-}^{195}Pt$ coupling of approximately 3800 Hz was observed in both spectra, showing unequivocally that coordination of phosphorus to the Pt(II) ion had occurred (Figure 2). The observation of a doublet in the ^{31}P NMR spectrum indicates only one phosphorus atom is coordinated to the Pt(II) ion in the product, while the ^{195}Pt NMR chemical shift of −3176 ppm, upfield from that of the starting material, is consistent with coordination of a soft donor atom to the Pt(II) ion.[13] The ^1H and ^{13}C NMR spectra strongly suggest that the two bpy ligands in the product are chemically equivalent on the NMR time scale. These observations are consistent with the formation of a 5-coordinate species in aqueous solution, which is either fluxional on the NMR time scale or in which the Pt(II) ion adopts a square pyramidal geometry that renders the two bpy ligands equivalent. Regardless of the geometry, the P donor atom remains bonded to the Pt(II) ion in solution. The ^1H diffusion-ordered spectroscopic (DOSY) NMR spectrum showed that

dx.doi.org/10.1021/ic403089j | Inorg. Chem. 2014, 53, 3595−3605

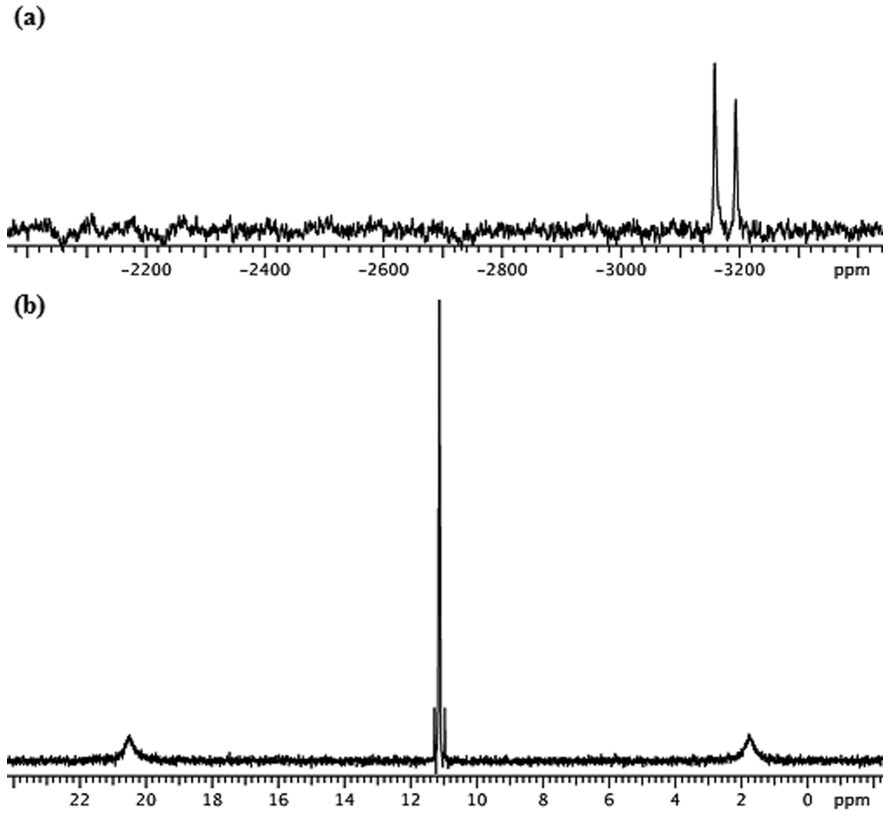

Figure 2. (a) ^{195}Pt (107 MHz) and (b) ^{31}P NMR (202 MHz) spectra of an equimolar mixture of $[Pt(bpy)_2](NO_3)_2{\cdot}H_2O$ and $K_2PPh(PPhSO_3)_2{\cdot}2H_2O$ in D_2O at 25 °C. ^1J coupling of approximately 3800 Hz between ^{195}Pt and ^{31}P was observed in both spectra, while ^1J coupling of 63.5 Hz between ^{31}P and ^{13}C was observed in the ^{31}P NMR spectrum.

the reaction of $[Pt(bpy)_2]^{2+}$ and $PPh(PhSO_3)_2^{2-}$ in D_2O gave a 1:1 adduct that has a diffusion coefficient of 2.72×10^{-10} m^2 s^{-1}, a much smaller value than those of the reactants ($[Pt(bpy)_2]^{2+}$, 4.23×10^{-10} m^2 s^{-1}; $PPh(PhSO_3)_2^{2-}$, 4.03×10^{-10} m^2 s^{-1}: Supporting Information, Figures S18, S19), indicative of the formation of a compound of higher molar mass. All of the NMR data are consistent with the formation of a 5-coordinate complex of the type $[Pt(bpy)_2\{PPh(PhSO_3)_2\}]$, in which the bpy ligands are equivalent. High-resolution mass spectral data also support the proposed formula, with peaks corresponding to $[Na(Pt(bpy)_2\{PPh(PhSO_3)_2\})]^+$ and $[K(Pt(bpy)_2\{PPh(PhSO_3)_2\})]^+$ observed at m/z = 950.0812 and 966.0387, respectively (Supporting Information, Figures S23, S24), as well as lower mass fragments derived from these.

The 5-coordinate nature of the product was confirmed by X-ray crystallography. Yellow, X-ray quality crystals of $[Pt(bpy)_2\{PPh(PhSO_3)_2\}]{\cdot}5.5H_2O$ were obtained by vapor diffusion of acetonitrile into an aqueous solution containing equimolar amounts of $[Pt(bpy)_2](NO_3)_2{\cdot}H_2O$ and $K_2PPh(PhSO_3)_2{\cdot}2H_2O$. Figure 3 shows an Oak Ridge thermal-ellipsoid plot (ORTEP) diagram of $[Pt(bpy)_2\{PPh(PhSO_3)_2\}]{\cdot}5.5H_2O$, with the waters of crystallization omitted for clarity. The neutral complex contains a central 5-coordinate Pt(II) ion that is bound to the N atoms of two chemically inequivalent bpy ligands and the P atom of a $PPh(PhSO_3)_2^{2-}$ ligand. The geometry about the Pt(II) ion is best described as distorted square pyramidal (τ_5 = 0.095)[18,19] with three N atoms (N1, N2, and N3) from the bpy ligands and the P atom from the $PPh(PhSO_3)_2^{2-}$ ligand defining the square plane. The Pt(II) ion sits very slightly (0.054 Å) above this plane. The "apex" of the square pyramid is occupied by the remaining N atom (N4) of a bpy ligand, although it is not positioned directly above the metal ion, as reflected in the N3−Pt1−N4 bond angle of 68.4°.

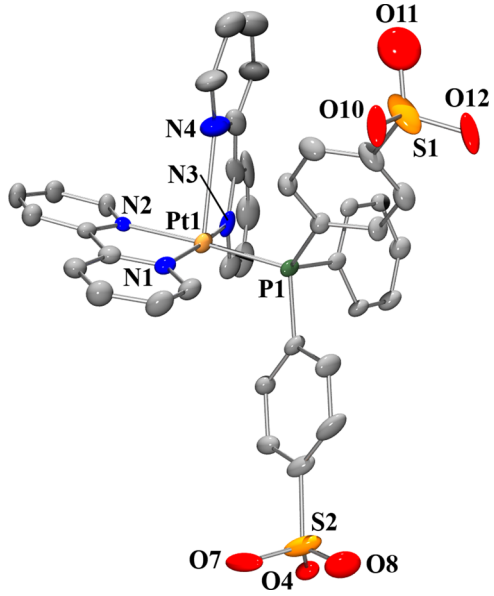

Figure 3. ORTEP diagram of $[Pt(bpy)_2\{PPh(PhSO_3)_2\}]{\cdot}5.5H_2O$; solvent water molecules and hydrogen atoms are omitted for clarity. Thermal ellipsoids are drawn at the 30% probability level. Selected bond lengths (Å) and angles (deg): Pt1−N1 2.049(9), Pt1−N2 2.092(8), Pt1−N3 2.050(11), Pt1−N4 2.753(14), Pt1−P1 2.260(2); N1−Pt1−N2 79.6(3), N1−Pt1−N3 170.9(4), N1−Pt1−P1 97.7(3), N2−Pt1−N3 92.1(3), N2−Pt1−P1 176.6(2), N3−Pt1−P1 90.5(2), N3−Pt1−N4 68.4(5).

dx.doi.org/10.1021/ic403089j | Inorg. Chem. 2014, 53, 3595−3605

Table 1. NMR Chemical Shifts of Phosphine Ligands, $[Pt(N{-}N)_2]^{2+}$, and $[Pt(N{-}N)_2(phosphine)]^{n+}$ Complexes

compound	solvent	^{31}P NMR δ, ppm ($^1J_{Pt-P}$, Hz)	^{195}Pt NMR δ, ppm ($^1J_{Pt-P}$, Hz)
$K_2PPh(PhSO_3)_2{\cdot}2H_2O$	D_2O	−6.79[a]	
PPh_3	CD_3OD	−4.74	
$[Pt(bpy)_2](NO_3)_2{\cdot}H_2O$	D_2O		−2270[b]
	CD_3OD		c,d
$[Pt(4,4'\text{-}Me_2bpy)_2](NO_3)_2{\cdot}2H_2O$	D_2O		−2242
	CD_3OD		c
$[Pt(bpy)_2\{PPh(PhSO_3)_2\}]$	D_2O	11.13 (3791)	−3176 (3805)
$[Pt(4,4'\text{-}Me_2bpy)_2\{PPh(PhSO_3)_2\}]$	D_2O	10.94 (3795)	−3197 (3795)
$[Pt(bpy)_2(PPh_3)](NO_3)_2$	CD_3OD	11.91 (3790)	c
$[Pt(4,4'\text{-}Me_2bpy)_2(PPh_3)](NO_3)_2$	CD_3OD	11.81 (3801)	c

[a]Reference 24 quotes −6.49 ppm. [b]From reference 13. [c]Insufficient solubility in this solvent to obtain a spectrum. [d]A 48 h data collection gives no ^{195}Pt NMR signal.

The Pt−N4 distance of 2.753 Å is also much longer than the Pt−N distances in the square plane (Pt1−N1, 2.049 Å; Pt1−N2, 2.092 Å; Pt1−N3, 2.050 Å), showing that one bpy ligand is bound very asymmetrically. A similar asymmetric binding of the phen ligand in $[Pt(phen)_2(CN)](NO_3){\cdot}H_2O$ has also been observed;[17] indeed, the coordination geometry about the Pt(II) ion in $[Pt(bpy)_2\{PPh(PhSO_3)_2\}]{\cdot}5.5H_2O$ is very similar to that found in $[Pt(phen)_2(CN)](NO_3){\cdot}H_2O$ (τ_5 = 0.045),[20] and such a coordination geometry has been predicted for the 5-coordinate $[Pt(bpy)_2(OH)]^+$ and $[Pt(bpy)_2(py)]^{2+}$ complexes by us[15] and Kawanishi et al.,[16] respectively, based on the results of DFT geometry optimization calculations. Although the bpy ligand, unlike the closely related phen ligand, possesses rotational freedom about the interannular C−C bond, the fact that N4 is oriented toward, rather than away from, the Pt(II) ion strongly suggests that there is a genuine bonding interaction (albeit weak) between Pt1 and N4 in $[Pt(bpy)_2\{PPh(PhSO_3)_2\}]{\cdot}5.5H_2O$. Note that this interaction is reproduced in the optimized structure obtained from DFT calculations (see below). The small dihedral angle (13.11°) between the pyridine rings of the asymmetrically bound bpy ligand is also consistent with both N atoms of the ligand being bonded to the Pt ion. A similar ligand orientation and long Pt−N distance (2.625(7) Å) is present in the terpyridine (terpy) ligand of the $[Pt(PNCHP\text{-}\kappa^3P,N,P)(terpy\text{-}\kappa^2N,N)]^{2+}$ cation,[21] while the peroxo-bridged dimer $[(bpy)_2Pt(\mu\text{-}O_2)Pt(bpy)_2](BF_4)_2$ also displays an asymmetrically coordinated bpy ligand.[22] However, in the latter compound, the dihedral angle between the pyridine rings of the nondisordered asymmetrically bound bpy ligand is 46.58°, and the corresponding "long" Pt−N distance is 2.975 Å. Both measurements, which are significantly larger than those in $[Pt(bpy)_2\{PPh(PhSO_3)_2\}]{\cdot}5.5H_2O$, are more consistent with a 4-coordinate square-planar geometry and are again suggestive of a genuine Pt1−N4 bonding interaction in $[Pt(bpy)_2\{PPh(PhSO_3)_2\}]{\cdot}5.5H_2O$.

Offset $\pi-\pi$ interactions[23] are observed in the crystal structure of $[Pt(bpy)_2\{PPh(PhSO_3)_2\}]{\cdot}5.5H_2O$. These occur between a phenyl ring of the $PPh(PhSO_3)_2^{2-}$ ligand and a pyridine ring of the asymmetrically bound bpy ligand (Supporting Information, Figure S37) and also between the symmetrically bound bpy ligands of two $[Pt(bpy)_2\{PPh(PhSO_3)_2\}]$ molecules (Supporting Information, Figure S38). The centroid−centroid distances are 3.723 and 3.669 Å, respectively.

Elemental analysis of the crystals used for the X-ray structural determination was consistent with the formula of $[Pt(bpy)_2\{PPh(PhSO_3)_2\}]{\cdot}5.5H_2O$. Dissolution of these crystals in D_2O gave the same ^1H NMR spectrum as that observed initially on mixing equimolar amounts of $[Pt(bpy)_2](NO_3)_2{\cdot}H_2O$ and $K_2PPh(PhSO_3)_2{\cdot}2H_2O$ in the same solvent. This observation suggests that, in contrast to the situation in the solid state, the two bpy ligands in the complex are equivalent in solution on the NMR time scale. We therefore propose that the complex is fluxional in solution.

Similar behavior to that described above is observed when $[Pt(4,4'\text{-}Me_2bpy)_2](NO_3)_2{\cdot}2H_2O$ is used as the starting material. NMR, UV−vis, and mass spectral studies of an aqueous solution containing equimolar amounts of $[Pt(4,4'\text{-}Me_2bpy)_2](NO_3)_2{\cdot}2H_2O$ and $K_2PPh(PhSO_3)_2{\cdot}2H_2O$ are consistent with formation of 5-coordinate $[Pt(4,4'\text{-}Me_2bpy)_2\{PPh(PhSO_3)_2\}]$. This complex shows slight decreases in the ^{31}P and ^{195}Pt NMR chemical shifts compared to those of $[Pt(bpy)_2\{PPh(PhSO_3)_2\}]$ (Table 1), presumably due to the more electron-rich 4,4′-Me_2bpy ligands, and it also appears to be somewhat less fluxional. The latter observation is supported by the presence of broad peaks in the ^1H NMR spectrum of $[Pt(4,4'\text{-}Me_2bpy)_2\{PPh(PhSO_3)_2\}]$ at 25 °C (Supporting Information, Figure S8), which sharpen significantly with increasing temperature (Supporting Information, Figure S9).

Synthesis and Characterization of $[Pt(N{-}N)_2(PPh_3)]^{2+}$ Complexes. The reaction of 1 equiv of PPh_3 with both $[Pt(bpy)_2]^{2+}$ and $[Pt(4,4'\text{-}Me_2bpy)_2]^{2+}$ in CH_3OH showed many similarities to those of $PPh(PhSO_3)_2^{2-}$ in aqueous solution described above, and 5-coordinate products were obtained with both Pt(II) starting materials. A bright yellow solution was formed on mixing equimolar amounts of $[Pt(N{-}N)_2](NO_3)_2$ and PPh_3, and chemical shifts different from those of the starting materials were observed in the ^1H and ^{13}C NMR spectra of these mixtures in CD_3OD (Supporting Information, Figures S11, S12, S18); these spectra also showed the N−N ligands to be chemically equivalent in solution. $^{31}P-^{195}Pt$ coupling of approximately 3800 Hz in the ^{31}P NMR spectra (Supporting Information, Figures S13, S15) gave evidence for coordination of the phosphorus atom of PPh_3 to the Pt(II) ion. Furthermore, the ^1H DOSY NMR spectra showed that the reaction of $[Pt(N{-}N)_2](NO_3)_2$ and PPh_3 in CD_3OD gave a product that has a diffusion coefficient of approximately 6×10^{-10} m^2 s^{-1}, consistent with formation of 5-coordinate $[Pt(N{-}N)_2(PPh_3)]^{2+}$ (Supporting Information, Figures S21, S22). Mass spectral evidence for the formation of $[Pt(N{-}N)_2(PPh_3)]^{2+}$ was also obtained (Supporting Information, Figures S29, S31). Unfortunately, despite many efforts, X-ray quality crystals of the products could not be obtained.

dx.doi.org/10.1021/ic403089j | Inorg. Chem. 2014, 53, 3595−3605

Table 2. X-ray Crystallographic Data for $[Pt(bpy)_2\{PPh(PhSO_3)_2\}]\cdot 5.5H_2O$ and $[Pt(bpy)(PPh_3)_2](ClO_4)_2\cdot 0.5(C_6H_{14}O)$

compound	$[Pt(bpy)_2\{PPh(PhSO_3)_2\}]\cdot 5.5H_2O$	$[Pt(bpy)(PPh_3)_2](ClO_4)_2\cdot 0.5(C_6H_{14}O)$
chemical formula	$C_{38}H_{40}N_4O_{11.5}PPtS_2$	$C_{49}H_{45}Cl_2N_2O_{8.5}P_2Pt$
formula weight	1026.92	1125.80
temperature, K	100.0(2)	100.0(1)
wavelength, Å	0.71070	0.71070
crystal system	monoclinic	monoclinic
space group	$P2_1/c$	$P2_1/c$
a, Å	11.8665(4)	10.4219(2)
b, Å	24.5917(7)	25.1945(6)
c, Å	15.8557(7)	18.9236(4)
α, deg	90	90
β, deg	103.382(4)	93.356(2)
γ, deg	90	90
volume, Å^3	4501.3(3)	4960.33(18)
Z	2	2
D_{calcd}, g cm^{-3}	1.515	1.508
μ, mm^{-1}	3.305	3.055
$R(F_o$ or $F_o^2)$	0.0836	0.0340
$R_w(F_o$ or $F_o^2)$	0.2358	0.0897

Formation of $[Pt^{II}(N-N)(phosphine)_2]^{n+}$ Complexes. The aqueous and methanolic solution studies show that the reactions of $[Pt(N-N)_2](NO_3)_2$ with 1 equiv of either phosphine ligand gives the 5-coordinate $[Pt(N-N)_2(phosphine)]^{n+}$ complexes quantitatively. The $[Pt(N-N)_2(phosphine)]^{n+}$ complexes are stable in solution for at least 4 d, as no significant spectral changes were observed in either the ^1H or ^{31}P NMR spectra over this time. However, while reaction of $[Pt(bpy)_2]^{2+}$ with 4 equiv of PPh_3 in CD_3OD also gave the 5-coordinate complex initially (Supporting Information, Figure S16), ^1H and ^{31}P NMR data gave evidence for the formation of a small amount (approximately 15%) of a new complex after one week. New NMR signals due to a very small amount of free bpy ligand were observed in the ^1H NMR spectrum recorded 22 h after sample preparation, and after one week, a new, small ^{31}P NMR signal was observed at 9.33 ppm. In analogous ^{31}P NMR studies with excess $K_2PPh(PhSO_3)_2\cdot 2H_2O$ in D_2O, a new singlet, flanked by ^{195}Pt satellites ($^{31}P-^{195}Pt$ coupling of 3498 Hz), was observed at 8.86 ppm. Given that $[Pt(bpy)_2]^{2+}$ is known to react with excess pyridine to give $[Pt(bpy)(py)_2]^{2+}$,[15] we suspected these new peaks might be due to the hitherto unknown complex $[Pt(bpy)(PPh_3)_2]^{2+}$. We therefore prepared $[Pt(bpy)(PPh_3)_2](ClO_4)_2$ by heating $[Pt(bpy)Cl_2]$ with 10 equiv of PPh_3 in a 1:2 H_2O/acetone mixture. Removal of unreacted PPh_3 and addition of $NaClO_4$ gave $[Pt(bpy)(PPh_3)_2](ClO_4)_2$ as an off-white solid. $[Pt(bpy)(PPh_3)_2](ClO_4)_2$ was characterized by elemental analysis, ^1H, ^{13}C, and ^{31}P NMR, mass spectroscopy, and X-ray crystallography. A single ^{31}P NMR signal at 8.80 ppm, flanked by ^{195}Pt satellites ($^{31}P-^{195}Pt$ coupling of 3560 Hz) was observed in the spectrum of $[Pt(bpy)(PPh_3)_2](ClO_4)_2$ in dimethylformamide (DMF)-d_7, suggesting that coordination of the phosphorus atom(s) of one or two PPh_3 ligand(s) to the Pt(II) ion had occurred (Supporting Information, Figure S5). In CD_3OD, the ^{31}P NMR signal appears as a broad singlet at 9.15 ppm. The formation of $[Pt(bpy)(PPh_3)_2]^{2+}$ is supported by high-resolution mass spectral data, with a peak corresponding to $[Pt(bpy)(PPh_3)_2]^{2+}$ observed at m/z = 437.6050 (Supporting Information, Figure S34).

The identity of $[Pt(bpy)(PPh_3)_2](ClO_4)_2$ was confirmed by X-ray crystallography (Table 2). Colorless, X-ray quality crystals of $[Pt(bpy)(PPh_3)_2](ClO_4)_2\cdot 0.5(C_6H_{14}O)$ were obtained by vapor diffusion of diisopropyl ether into a solution of $[Pt(bpy)(PPh_3)_2](ClO_4)_2$ in acetone. Figure 4 shows a diagram of the $[Pt(bpy)(PPh_3)_2]^{2+}$ cation. This consists of a central 4-coordinate Pt(II) ion that is bound to both N atoms of a bpy ligand and the P atoms of two PPh_3 ligands. The geometry about the Pt(II) ion is best described as distorted square planar (τ_4 = 0.19);[25] the two P donor atoms sit on either side of the plane defined by Pt1, N1, and N2,[26] while there is a significant bowing in the bpy ligand. Presumably, the observed geometry about the Pt(II) ion minimizes the unfavorable intra- or interligand proton−proton interactions. In addition, this geometry allows an interligand, offset $\pi-\pi$ interaction between phenyl rings of the two PPh_3 ligands, with a centroid−centroid distance of 3.531 Å (Supporting Information, Figure S39). No $\pi-\pi$ interactions between the bpy ligands of neighboring $[Pt(bpy)(PPh_3)_2]^{2+}$ cations are observed, presumably due to the close proximity of two sterically demanding PPh_3 ligands

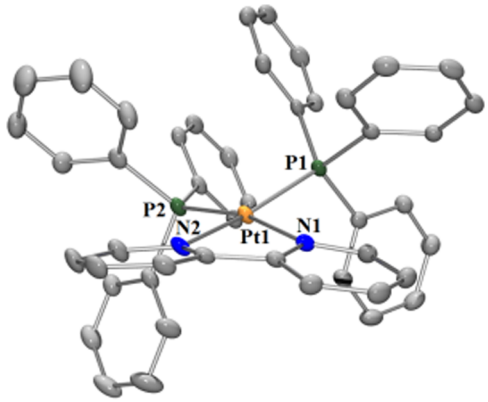

Figure 4. ORTEP diagram of the $[Pt(bpy)(PPh_3)_2]^{2+}$ cation; hydrogen atoms are omitted for clarity. Thermal ellipsoids are drawn at the 50% probability level. Selected bond lengths (Å) and angles (deg): Pt1−N1 2.102(3), Pt1−N2 2.110(3), Pt1−P1 2.2753(8), Pt1−P2 2.2849(9); N1−Pt1−N2 77.97(11), N1−Pt1−P2 167.29(8), N1−Pt1−P1 94.34(8), N2−Pt1−P2 94.50(8), N2−Pt1−P1 166.30(9), P1−Pt1−P2 94.96(3).

dx.doi.org/10.1021/ic403089j | Inorg. Chem. 2014, 53, 3595−3605

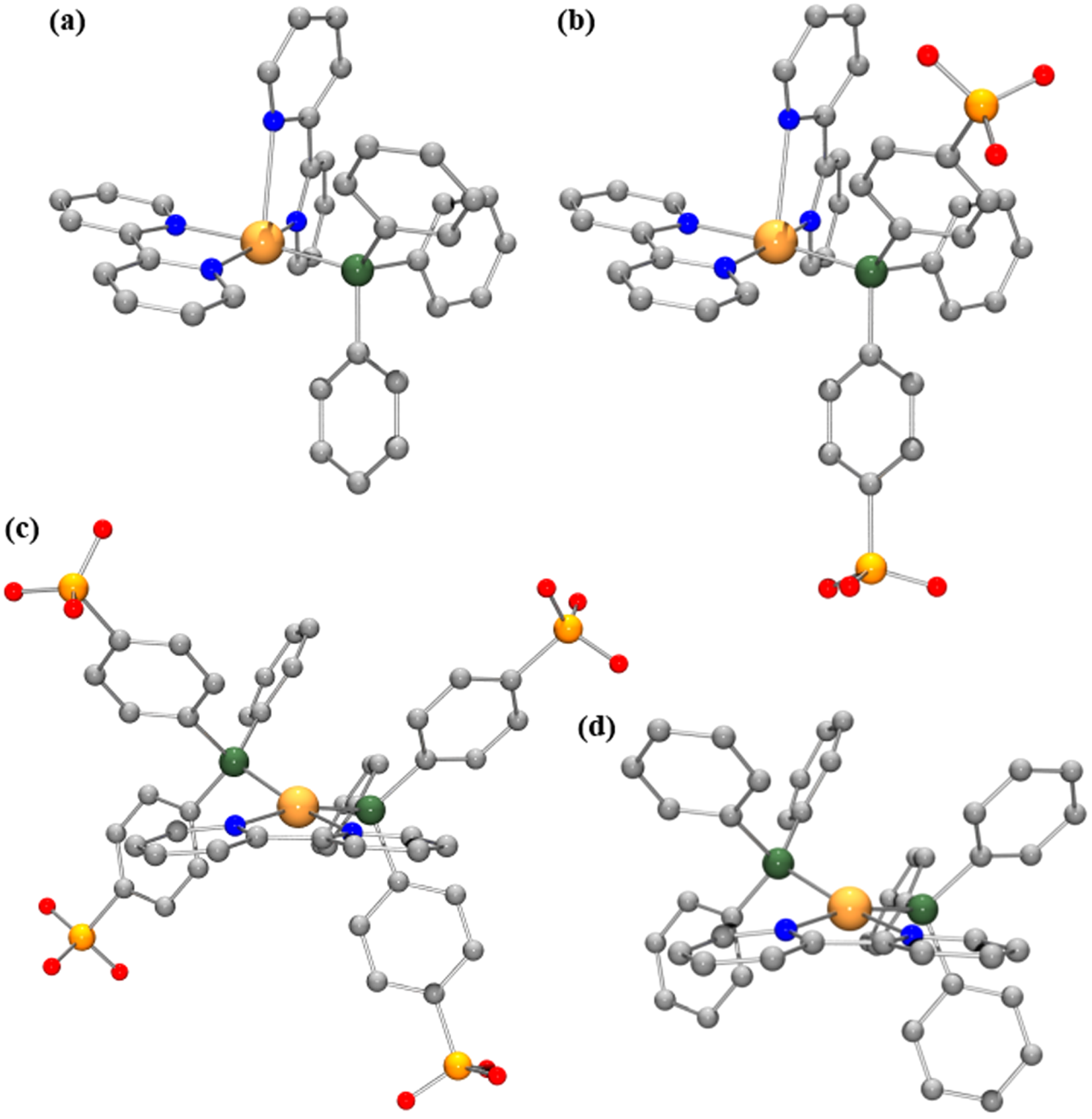

Figure 5. Ball-and-stick representations of optimized structures of (a) $[Pt(bpy)_2(PPh_3)]^{2+}$, (b) $[Pt(bpy)_2\{PPh(PhSO_3)_2\}]$, (c) $[Pt(bpy)\{PPh(PhSO_3)_2\}_2]^{2-}$, and (d) $[Pt(bpy)(PPh_3)_2]^{2+}$ from density functional calculations; hydrogen atoms are omitted for clarity. Color scheme for each element: C (gray), N (blue), O (red), P (dark green), Pt (gold), and S (orange).

and a perchlorate anion (Supporting Information, Figure S40). Interestingly, anion-π interactions[27] are observed between a bpy ligand and the perchlorate anion oxygen atoms O5 and O8 (Supporting Information, Figure S41), with the oxygen−centroid distances being 3.161 and 2.947 Å, respectively. The Pt−N distances of 2.102 Å (Pt1−N1) and 2.110 Å (Pt1−N2) are rather longer than those in $[Pt^{II}(bpy)_2]X$ (X = $(NO_3)_2\cdot H_2O$, $(ClO_4)_2$, $(CF_3SO_3)_2$, $\{Au(CN)_2\}_2$, $[C_6H_4\{C(CN)_2\}_2]_2$),[28−33] consistent with the significant trans effect exerted by phosphine ligands.

The similarity in ^{31}P NMR chemical shifts between $[Pt(bpy)(PPh_3)_2]^{2+}$ (9.15 ppm) and the unknown peak (9.33 ppm) in CD_3OD strongly suggests that the unknown peak is indeed due to $[Pt(bpy)(PPh_3)_2]^{2+}$, while the peak observed in the aqueous spectrum (8.86 ppm) is due to $[Pt(bpy)\{PPh(PhSO_3)_2\}_2]^{2-}$. This makes intuitive sense, as the asymmetrically bonded bpy ligand in 5-coordinate $[Pt(bpy)_2(phosphine)]^{n+}$ might be expected to be relatively easily substituted. Note also that the ^{31}P NMR data are not consistent with formation of the recently characterized cyclometalated complex $[Pt(bpy\text{-}H\text{-}\kappa N,C)(PPh_3)_2]^+$.[34]

Mechanism of the Reaction of $[Pt(bpy)_2]^{2+}$ with Phosphine Ligands. Extensive studies of the mechanism of ligand substitution in square planar Pt(II) complexes have shown this process to have associative character, with only a few exceptions.[35,36] Our study of the reaction of $[Pt(N{-}N)_2]^{2+}$ with phosphine ligands provides support for the associative ligand substitution mechanism. NMR studies clearly show that

dx.doi.org/10.1021/ic403089j | Inorg. Chem. 2014, 53, 3595−3605

Table 3. Comparison of Calculated and Observed Structural Data for $[Pt(bpy)_2]^{2+}$, $[Pt^{II}(bpy)_2(phosphine)]^{n+}$, and $[Pt^{II}(bpy)(phosphine)_2]^{n+}$ Complexes

complex	calculated Pt−N (Å)	experimental Pt−N (Å)	calculated Pt−P (Å)	experimental Pt−P (Å)
$[Pt(bpy)_2]^{2+}$	2.039, 2.039, 2.039, 2.040	2.023, 2.023, 2.029, 2.029		
$[Pt(bpy)_2(PPh_3)]^{2+}$	2.055, 2.068, 2.114, 2.758		2.310	
$[Pt(bpy)(PPh_3)_2]^{2+}$	2.136, 2.154	2.102, 2.110	2.322, 2.328	2.275, 2.285
$[Pt(bpy)_2\{PPh(PhSO_3)_2\}]$	2.054, 2.068, 2.109, 2.753	2.049, 2.050, 2.092, 2.753	2.311	2.260
$[Pt(bpy)\{PPh(PhSO_3)_2\}_2]^{2-}$	2.130, 2.151		2.321, 2.330	

the reaction of $[Pt(N{-}N)_2]^{2+}$ with excess phosphine ligand [PPh_3 or $PPh(PhSO_3)_2^{2-}$] immediately gives quantitative formation of the 5-coordinate $[Pt(N{-}N)_2(phosphine)]^{n+}$ complex as a long-lived intermediate, with subsequent rate-determining entry of a further phosphine ligand to give $[Pt(N{-}N)(phosphine)_2]^{n+}$ as the final product. The driving force for entry of the first phosphine ligand appears to be relief of steric strain in the $[Pt(N{-}N)_2]^{2+}$ starting material. Close approach of the 6 and 6′ bpy protons in the square planar starting material results in either a bowing of the bpy ligands[30−33] or a slight distortion toward tetrahedral geometry[29] in the solid state. Such unfavorable interactions are not observed in the crystal structure of $[Pt(bpy)_2\{PPh(PhSO_3)_2\}]\cdot 5.5H_2O$, with the symmetrically bound bpy ligand being essentially planar. It is likely that this is also the basis of the facile reaction of $[Pt(N{-}N)_2]^{2+}$ with OH^-, other anions, and aromatic nitrogen bases.

Calculations on $[Pt(bpy)_2]^{2+}$, $[Pt^{II}(bpy)_2(phosphine)]^{n+}$, and $[Pt^{II}(bpy)(phosphine)_2]^{n+}$. Density functional calculations were carried out to optimize the geometries of $[Pt(bpy)_2]^{2+}$, $[Pt(bpy)_2(phosphine)]^{n+}$, and $[Pt(bpy)(phosphine)_2]^{n+}$ (Figure 5). Comparisons of computational and available experimental data for these complexes are given in Table 3. The calculated structures of $[Pt(bpy)_2]^{2+}$, $[Pt(bpy)_2\{PPh(PhSO_3)_2\}]$, and $[Pt(bpy)(PPh_3)_2]^{2+}$ are in good agreement with the corresponding crystal structures; the Pt(II) ion displays a perfect square planar geometry in $[Pt(bpy)_2]^{2+}$, a distorted square pyramidal geometry in $[Pt(bpy)_2(phosphine)]^{n+}$, and a distorted square planar geometry in $[Pt(bpy)(phosphine)_2]^{n+}$. In addition, interligand $\pi{-}\pi$ interactions between the phenyl rings of the two phosphine ligands and between a phenyl ring of a phosphine ligand and a pyridine ring of the asymmetrically bound bpy ligand are observed in the calculated structures of $[Pt(bpy)(phosphine)_2]^{n+}$ and $[Pt(bpy)_2(phosphine)]^{n+}$, respectively. Of particular importance are the computational results for both 5-coordinate complexes, which are predicted to have a distorted square pyramidal geometry with a bpy N atom in the apical position; indeed, no convergence could be obtained when the P atom of the phosphine ligand was placed in this position. Thus, it is very likely that the observed equivalence of the bpy ligands of these complexes in solution is due to a fluxional process involving interconversion of species having bpy N atoms at the apical position of a square pyramid, rather than the bpy ligands themselves being truly equivalent.

The calculated bonding energy results for $[Pt(bpy)_2]^{2+}$, $[Pt(bpy)_2(phosphine)]^{n+}$, and $[Pt(bpy)(phosphine)_2]^{2+}$ provide some insight into the driving force for the formation of $[Pt(bpy)(phosphine)_2]^{n+}$ from $[Pt(bpy)_2]^{2+}$. The bonding energy data listed in Table 4 show that the trend in thermodynamic stability is $[Pt(bpy)_2]^{2+} < [Pt(bpy)_2(phosphine)]^{n+} < [Pt(bpy)(phosphine)_2]^{2+}$, and thus the final product $[Pt(bpy)(phosphine)_2]^{2+}$ is the most energetically favored species.

Table 4. Calculated Bonding Energy Data for $[Pt(bpy)_2]^{2+}$, $[Pt^{II}(bpy)_2(phosphine)]^{n+}$, and $[Pt^{II}(bpy)(phosphine)_2]^{n+}$ Complex−Ligand Systems

complex−ligand system	bonding energy (kJ mol^{-1})
$[Pt(bpy)_2]^{2+} + 2PPh_3$	−67 604
$[Pt(bpy)_2(PPh_3)]^{2+} + PPh_3$	−67 620
$[Pt(bpy)(PPh_3)_2]^{2+} + bpy$	−67 629
$[Pt(bpy)_2]^{2+} + 2PPh(PhSO_3)_2^{2-}$	−76 885
$[Pt(bpy)_2\{PPh(PhSO_3)_2\}] + PPh(PhSO_3)_2^{2-}$	−76 910
$[Pt(bpy)\{PPh(PhSO_3)_2\}_2]^{2-} + bpy$	−76 913

The bonding energy data in Table 4 can also be used to calculate the energy change (ΔE) for the formation of $[Pt(bpy)_2(phosphine)]^{n+}$ and $[Pt(bpy)(phosphine)_2]^{n+}$ complexes, and the results are summarized in Scheme 3. These results show that the formation of both $[Pt(bpy)_2(phosphine)]^{n+}$ and $[Pt(bpy)(phosphine)_2]^{n+}$ complexes is characterized by favorable energetics. Interestingly, the formation of $[Pt(bpy)_2(phosphine)]^{n+}$ is predicted to be more energetically favorable when $PPh(PhSO_3)_2^{2-}$ is the ligand, whereas PPh_3 is the preferred ligand in the formation of $[Pt(bpy)(phosphine)_2]^{n+}$.

The isolation of $[Pt(bpy)_2\{PPh(PhSO_3)_2\}]\cdot 5.5H_2O$ and NMR solution studies clearly show that $[Pt(bpy)_2(phosphine)]^{n+}$ forms rapidly as a stable reaction intermediate, and this observation is supported by the results from bonding energy calculations. These calculations suggest that the formation of $[Pt(bpy)(phosphine)_2]^{n+}$ from $[Pt(bpy)_2(phosphine)]^{n+}$ is also an energetically favorable process. The formation of $[Pt(bpy)(phosphine)_2]^{n+}$ has been observed in solution NMR studies, and this process has been shown to occur much more slowly than the formation of $[Pt(bpy)_2(phosphine)]^{n+}$ from $[Pt(bpy)_2]^{2+}$. One reason is that both decoordination of a bidentate bpy ligand and coordination of a sterically bulky phosphine ligand are required in the formation of $[Pt(bpy)(phosphine)_2]^{n+}$; however, only the coordination of a phosphine ligand is required in the formation of $[Pt(bpy)_2(phosphine)]^{n+}$. Furthermore, the Pt(II) ion in $[Pt(bpy)_2(phosphine)]^{n+}$ is less exposed to the incoming phosphine ligand than that in $[Pt(bpy)_2]^{2+}$, and therefore, a larger degree of preorganization between $[Pt(bpy)_2(phosphine)]^{n+}$ and the incoming phosphine ligand is required in the formation of $[Pt(bpy)(phosphine)_2]^{n+}$. As a result, the formation of $[Pt(bpy)(phosphine)_2]^{n+}$ is much slower than that of $[Pt(bpy)_2(phosphine)]^{n+}$.

CONCLUSIONS

This work provides the first definitive X-ray structural evidence, in the form of $[Pt(bpy)_2\{PPh(PhSO_3)_2\}]\cdot 5.5H_2O$, for the formation of 5-coordinate species from the reaction of $[Pt(N{-}N)_2]^{2+}$ (N−N = bpy, 4,4′-Me_2bpy) complexes with monodentate ligands in both aqueous and methanolic solution. Such

dx.doi.org/10.1021/ic403089j | Inorg. Chem. 2014, 53, 3595−3605

Scheme 3. Formation Reaction Energetics (ΔE) of $[Pt^{II}(bpy)_2(phosphine)]^{n+}$ and $[Pt^{II}(bpy)(phosphine)_2]^{n+}$ Complexes

$$[Pt(bpy)_2]^{2+} + 2\ PPh_3 \longrightarrow [Pt(bpy)_2(PPh_3)]^{2+} + PPh_3 \qquad \Delta E = -16\ kJ\ mol^{-1}$$

$$[Pt(bpy)_2(PPh_3)]^{2+} + PPh_3 \longrightarrow [Pt(bpy)(PPh_3)_2]^{2+} + bpy \qquad \Delta E = -9\ kJ\ mol^{-1}$$

$$[Pt(bpy)_2]^{2+} + 2\ PPh(PhSO_3)_2^{2-} \longrightarrow [Pt(bpy)_2\{PPh(PhSO_3)_2\}] + PPh(PhSO_3)_2^{2-} \qquad \Delta E = -25\ kJ\ mol^{-1}$$

$$[Pt(bpy)_2\{PPh(PhSO_3)_2\}] + PPh(PhSO_3)_2^{2-} \longrightarrow [Pt(bpy)\{PPh(PhSO_3)_2\}_2]^{2-} + bpy \qquad \Delta E = -3\ kJ\ mol^{-1}$$

5-coordinate species are formed rapidly and show significant stability in both the solid state and solution. Subsequent slow reaction of these with excess ligand gives $[Pt(N{-}N)(phosphine)_2]^{2+}$ as the final product. These observations confirm an associative substitution mechanism for these reactions. It would be remarkable if the formation of 5-coordinate complexes was limited to phosphine ligands, and it appears very likely that previously studied heterocyclic nitrogenous base and anionic ligands react similarly to give 5-coordinate complexes. Of arguably greatest interest, and certainly greatest controversy, among these is OH^-, and the results presented above provide more evidence, in addition to that already collected,[15] for coordination of this ligand to the Pt^{2+} ion in $[Pt(N{-}N)_2]^{2+}$ to give 5-coordinate $[Pt(N{-}N)_2(OH)]^+$. Most notably, we have shown that the UV–vis spectral changes that occur on formation of the structurally characterized 5-coordinate species $[Pt(bpy)_2\{PPh(PhSO_3)_2\}]$ in aqueous solution are very similar to those observed in the reaction of $[Pt(bpy)_2]^{2+}$ and OH^-.

EXPERIMENTAL SECTION

General Methods. Deuterated solvents were degassed with argon gas. Unless otherwise stated, all NMR spectra were recorded at 25 °C. ^1H and ^{13}C NMR spectra, and two-dimensional gradient correlation spectroscopy (gCOSY), total correlated spectroscopy (TOCSY), DOSY, heteronuclear single quantum coherence adiabatic (HSQCAD), and gradient-selected heteronuclear multiple bond correlation using adiabatic pulses (gHMBCAD) NMR spectra, were recorded on either a Varian 400-MR or Varian 500 MHz AR spectrometer. ^{31}P NMR spectra were recorded on either a Varian 400-MR or Varian 500 MHz AR spectrometer at 162 and 202 MHz, respectively. ^{195}Pt NMR spectra were recorded on a Varian 500 MHz AR spectrometer at 107 MHz. All chemical shifts are reported in parts per million (ppm). ^1H and ^{13}C NMR chemical shifts are referenced to internal standard NaTSP-d_4 (in D_2O: ^1H δ 0 ppm, ^{13}C δ 0 ppm) or tetramethylsilane (TMS) (in CD_3OD, dimethyl sulfoxide (DMSO)-d_6, or DMF-d_7: ^1H δ 0 ppm, ^{13}C δ 0 ppm). ^{31}P NMR chemical shifts are reported relative to an external reference of aqueous H_3PO_4 (40 wt %) at 0 ppm. ^{195}Pt NMR chemical shifts are reported relative to $H_2[PtCl_6]$ at 0 ppm, via an external reference of aqueous $K_2[PtCl_4]$ (0.1 M in 1 M DCl; −1620 ppm relative to $H_2[PtCl_6]$). High-resolution electrospray ionization mass spectra (HRESI-MS) were recorded on a Bruker micrOTOF-Q spectrometer. UV–vis absorption spectra were recorded at room temperature on a Perkin-Elmer Lambda 950 UV–vis–near-IR spectrophotometer. Elemental analyses were performed at the Campbell Microanalytical Laboratory, University of Otago.

Reagents. All regents were laboratory reagent grade or better and used as received. Dipotassium bis(*p*-sulfonatophenyl)phenylphosphine dihydrate ($K_2PPh(PhSO_3)_2{\cdot}2H_2O$) was purchased from Sigma-Aldrich and used as received. However, while characterizing this commercial product, we found some discrepancies in the NMR data reported in the literature. Reference 37 reports correct ^{13}C NMR data for this compound, but the reported ^{31}P NMR data are incorrect. The latter are correctly reported in reference 32, but neither reference reports ^1H NMR data. We do so below.

$K_2PPh(PhSO_3)_2{\cdot}2H_2O$. HRESI-MS (positive mode, MeOH): m/z calcd for $C_{18}H_{13}K_2NaO_6PS_2^+$: 520.9058 $[K_2PPh(PhSO_3)_2 + Na]^+$ ($[M + Na]^+$); found 520.9067 (96%), m/z calcd for $C_{18}H_{13}KNa_2O_6PS_2^+$: 504.9318 $[M - K + 2Na]^+$; found 504.9308 (100%), m/z calcd for $C_{18}H_{13}Na_3O_6PS_2^+$: 488.9579 $[M - 2K + 3Na]^+$; found 488.9563 (52%). ESI-MS (negative mode, MeOH): m/z calcd for $C_{18}H_{13}KO_6PS_2^-$: 458.9534 ($[M - K]^-$); found 458.9595 (12%), m/z calcd for $C_{18}H_{13}O_6PS_2^{2-}$: 209.9951 ($[M - 2K]^{2-}$); found 210.0002 (100%). ^1H NMR (500 MHz, D_2O): 7.76–7.81 (m, 4H, H_c), 7.39–7.51 (m, 9H, H_b, H_f, H_g, H_h). ^{13}C NMR (126 MHz, D_2O): 145.9 (s, C_d), 142.9 (d, $^1J_{P-C}$ = 9.5 Hz, C_a), 137.5 (d, $^1J_{P-C}$ = 6.3 Hz, C_e), 136.9 (d, $^2J_{P-C}$ = 20.0 Hz, C_f), 136.8 (d, $^2J_{P-C}$ = 19.2 Hz, C_b), 132.8 (s, C_h), 132.0 (d, $^3J_{P-C}$ = 7.7 Hz, C_g), 128.4 (d, $^3J_{P-C}$ = 7.1 Hz, C_c). ^{31}P NMR (202 MHz, D_2O): −6.79 (s with satellites; $^2J_{P-C}$ = 19.0 Hz).

Syntheses. $[Pt(bpy)Cl_2]$,[38] $[Pt(bpy)_2](ClO_4)_2$,[39] and $[Pt(bpy)_2](NO_3)_2{\cdot}H_2O$[13] were synthesized by reported methods.

Caution! *Although no difficulties were experienced with the perchlorate salts described herein, all perchlorate species should be treated as potentially explosive and handled with care.*

$[Pt(bpy)_2](NO_3)_2{\cdot}H_2O$.[13] To a stirred suspension of $[Pt(bpy)_2](ClO_4)_2$ (4.44 g, 6.29 mmol) in H_2O (200 mL) was added dropwise an aqueous solution of $[AsPh_4]Cl{\cdot}H_2O$ (5.50 g, 12.6 mmol) in H_2O (20 mL). $[AsPh_4]ClO_4$ precipitated immediately as a white solid. The mixture was first stirred at room temperature for 15 min and then on an ice-bath for 10 min; the solid was then removed by filtration through Celite and washed with ice-cold H_2O (2 × 10 mL). The yellow filtrate was concentrated (by rotary evaporator (rotavap)) to low volume (ca. 40 mL) and passed through a column of Dowex anion exchange resin (100–200 mesh size, NO_3^- form), and the yellow eluate was taken to dryness (rotavap) to give a yellow solid, which was washed with ice-cold H_2O (2 × 5 mL), then acetone (3 × 10 mL), and finally diethyl ether (3 × 10 mL) and dried under vacuum. Yield: 3.75 g (92%). Anal. Calcd (%) for $C_{20}H_{18}N_6O_7Pt$: C 36.99, H 2.79, N 12.94; found C 37.27, H 2.88, N 12.93. HRESI-MS (MeCN): m/z calcd for $C_{20}H_{16}N_5O_3Pt^+$: 569.0897 $[M + NO_3]^+$; found 569.0859 (2%), m/z calcd for $C_{21}H_{16}N_5Pt^+$: 533.1049 $[M + CN]^+$; found 533.1008 (58%), m/z calcd for $C_{20}H_{15}N_4Pt^+$: 506.0941 $[M - H]^+$; found 506.0897 (38%), m/z calcd for $C_{20}H_{16}N_4Pt^{2+}$: 253.5507 $[Pt(bpy)_2]^{2+}$ ($[M]^{2+}$); found 253.5503 (9%), m/z calcd for $C_{10}H_9N_2^+$: 157.0760 $[bpy + H]^+$; found 157.0804 (100%). ^1H NMR (400 MHz, DMSO-d_6): 9.10 (d, J = 5.5 Hz, 4H, bpyH-6/6′), 8.85 (dd, J = 8.1, 1.1 Hz, 4H, bpyH-3/3′), 8.64 (td, J = 8.0, 1.0 Hz, 4H, bpyH-4/4′), 7.99–8.10 (m, 4H, bpyH-5/5′). ^1H NMR (500 MHz, D_2O): 8.96 (d, J = 5.8 Hz, 4H, bpyH-6/6′), 8.51–8.61 (m, 8H, bpyH-3/3′, bpyH-4/4′), 7.90–8.03 (m, 4H, bpyH-5/5′). ^{13}C NMR (101 MHz, DMSO-d_6): 156.6 (bpyC-2/2′), 151.6 (bpyC-6/6′), 142.6 (bpyC-4/4′), 128.6 (bpyC-5/5′), 124.7 (bpyC-3/3′). ^{13}C NMR (101 MHz, D_2O): 159.9 (bpyC-2/2′), 153.6 (bpyC-6/6′), 145.8 (bpyC-4/4′), 131.3 (bpyC-5/5′), 127.6 (bpyC-3/3′).

The 4,4′-dimethyl substituted complexes $[Pt(4,4'\text{-}Me_2bpy)Cl_2]$, $[Pt(4,4'\text{-}Me_2bpy)_2](ClO_4)_2$, and $[Pt(4,4'\text{-}Me_2bpy)_2](NO_3)_2{\cdot}2H_2O$ were synthesized by methods analogous to those used for the nonsubstituted bpy complexes. The syntheses of $[Pt(4,4'\text{-}Me_2bpy)Cl_2]$ and $[Pt(4,4'\text{-}Me_2bpy)_2](ClO_4)_2$ are given in the Supporting Information.

$[Pt(4,4'\text{-}Me_2bpy)_2](NO_3)_2{\cdot}2H_2O$. An aqueous solution of $[AsPh_4]Cl{\cdot}H_2O$ (2.67 g, 6.11 mmol) in H_2O (30 mL) was added dropwise to a stirred suspension of $[Pt(4,4'\text{-}Me_2bpy)_2](ClO_4)_2$ (2.33 g, 3.06 mmol) in H_2O (70 mL). $[AsPh_4]ClO_4$ precipitated immediately as a white

dx.doi.org/10.1021/ic403089j | Inorg. Chem. 2014, 53, 3595–3605

solid. The mixture was first stirred at room temperature for 20 min and then on an ice-bath for 10 min; the solid was then removed by filtration through Celite and washed with ice-cold H_2O (2 × 25 mL). The resulting yellow filtrate was passed through a column of Dowex anion exchange resin (100−200 mesh size, NO_3^- form), and the yellow eluate was taken to dryness (rotavap) to give a yellow solid, which was washed with ice-cold H_2O (2 × 3 mL), then acetone (2 × 4 mL), and finally diethyl ether (3 × 10 mL) and dried under vacuum. Yield: 2.11 g (95%). Anal. Calcd (%) for $C_{24}H_{28}N_6O_8Pt$: C 39.84, H 3.90, N 11.61; found C 39.71, H 3.90, N 11.43. HRESI-MS (MeCN): *m/z* calcd for $C_{24}H_{24}N_5O_3Pt^+$: 625.1523 $[M + NO_3]^+$; found 625.1507 (6%), *m/z* calcd for $C_{25}H_{24}N_5Pt^+$: 589.1676 $[M + CN]^+$; found 589.1675 (70%), *m/z* calcd for $C_{24}H_{24}N_4Pt^{2+}$: 281.5820 $[Pt(4,4'\text{-}Me_2bpy)_2]^{2+}$ $([M]^{2+})$; found 281.5839 (100%). ^1H NMR (400 MHz, DMSO-d_6): 8.89 (d, *J* = 6.2 Hz, 4H, bpyH-6/6′), 8.69 (s, 4H, bpyH-3/3′), 7.85 (d, *J* = 5.5 Hz, 4H, bpyH-5/5′), 2.66 (s, 12H, CH_3). ^1H NMR (400 MHz, D_2O): 8.61 (d, *J* = 6.1 Hz, 4H, bpyH-6/6′), 8.25 (s, 4H, bpyH-3/3′), 7.64 (d, *J* = 5.9 Hz, 4H, bpyH-5/5′), 2.70 (s, 12H, CH_3). ^{13}C NMR (101 MHz, D_2O): 159.5 (bpyC-4/4′), 158.8 (bpyC-2/2′), 152.3 (bpyC-6/6′), 132.0 (bpyC-5/5′), 128.1 (bpyC-3/3′), 23.9 (CH_3). ^{195}Pt NMR (107 MHz, D_2O): −2242 ppm.

In Situ Synthesis of $[Pt(bpy)_2\{PPh(PhSO_3)_2\}]$ in D_2O Solution. A yellow solution of $[Pt(bpy)_2](NO_3)_2\cdot H_2O$ in D_2O (32 mM, 0.361 mL) was added to a colorless solution of $K_2PPh(PhSO_3)_2\cdot 2H_2O$ in D_2O (32 mM, 0.361 mL) at room temperature to give a more intense yellow solution containing $[Pt(bpy)_2\{PPh(PhSO_3)_2\}]$. HRESI-MS (MeCN): *m/z* calcd for $C_{38}H_{29}KN_4O_6PPtS_2^+$: 966.0548 $[(Pt(bpy)_2\{PPh(PhSO_3)_2\}) + K]^+$ $([M + K]^+)$; found 966.0387 (12%), *m/z* calcd for $C_{38}H_{29}N_4NaO_6PPtS_2^+$: 950.0809 $[M + Na]^+$; found 950.0812 (13%), *m/z* calcd for $C_{22}H_{18}N_4NaO_4Pt^+$: 620.0870 $[M - PPh(PhSO_3)_2 + 2O_2CH + Na]^+$; found 620.0828 (100%), *m/z* calcd for $C_{38}H_{29}N_4Na_2O_6PPtS_2^{2+}$: 486.5350 $[M + 2Na]^{2+}$; found 486.5316 (10%). ^1H NMR (500 MHz, D_2O): 8.27−8.39 (m, 4H, bpyH-6/6′), 8.24 (d, *J* = 8.0 Hz, 4H, bpyH-3/3′), 8.18 (td, *J* = 7.9, 1.4 Hz, 4H, bpyH-4/4′), 7.67−7.77 (m, 6H, H_f, H_c), 7.65 (td, *J* = 7.6, 7.1, 1.6 Hz, 1H, H_h), 7.53−7.62 (m, 4H, H_b), 7.44 (m, 6H, bpyH-5/5′, H_g). ^{13}C NMR (126 MHz, D_2O): 158.5 (s, bpyC-2/2′), 154.3 (s, bpyC-6/6′), 149.3 (d, $^4J_{C-P}$ = 2.9 Hz, C_d), 144.2 (s, bpyC-4/4′), 137.4−137.7 (m, C_b, C_f), 136.3 (d, $^4J_{C-P}$ = 2.7 Hz, C_h), 132.5 (d, $^3J_{C-P}$ = 12.0 Hz, C_g), 130.6 (s, bpyC-5/5′), 130.3 (d, $^1J_{C-P}$ = 63.3 Hz, C_a), 129.0 (d, $^3J_{C-P}$ = 12.0 Hz, C_c), 128.5 (s, bpyC-3/3′), 125.3 (d, $^1J_{C-P}$ = 64.0 Hz, C_e). ^{31}P NMR (202 MHz, D_2O): 11.13 (s with satellites; $^1J_{P-Pt}$ = 3791 Hz, $^1J_{P-C}$ = 63.5 Hz and $^2J_{P-C}$ = 11.8 Hz). ^{195}Pt NMR (107 MHz, D_2O): −3176 (d, $^1J_{Pt-P}$ = 3805 Hz).

Synthesis of $[Pt(bpy)_2\{PPh(PhSO_3)_2\}]\cdot 5.5H_2O$. Yellow crystals of $[Pt(bpy)_2\{PPh(PhSO_3)_2\}]\cdot 5.5H_2O$ suitable for X-ray crystallography were obtained by vapor diffusion of MeCN into an equimolar mixture of $[Pt(bpy)_2](NO_3)_2\cdot H_2O$ and $K_2PPh(PhSO_3)_2\cdot 2H_2O$ in aqueous solution over a period of 10 d. Anal. Calcd (%) for $C_{38}H_{40}N_4O_{11.5}PPtS_2$: C 44.44, H 3.93, N 5.46, S 6.24; found: C 44.32, H 3.59, N 5.61, S 6.48.

In Situ Synthesis of $[Pt(4,4'\text{-}Me_2bpy)_2\{PPh(PhSO_3)_2\}]$ in D_2O Solution. A yellow solution of $[Pt(4,4'\text{-}Me_2bpy)_2](NO_3)_2\cdot 2H_2O$ in D_2O (10 mM, 0.790 mL) was added to $K_2PPh(PhSO_3)_2\cdot 2H_2O$ (4.2 mg, 7.9 μmol). The mixture was stirred at room temperature until the $K_2PPh(PhSO_3)_2\cdot 2H_2O$ dissolved, giving a more intense yellow solution containing $[Pt(4,4'\text{-}Me_2bpy)_2\{PPh(PhSO_3)_2\}]$. HRESI-MS (MeCN): *m/z* calcd for $C_{42}H_{37}KN_4O_6PPtS_2^+$: 1022.1175 $[(Pt(4,4'\text{-}Me_2bpy)_2\{PPh(PhSO_3)_2\}) + K]^+$ $([M + K]^+)$; found 1022.1203 (3%), *m/z* calcd for $C_{42}H_{37}N_4NaO_6PPtS_2^+$: 1006.1435 $[M + Na]^+$; found 1006.1486 (3%), *m/z* calcd for $C_{42}H_{38}N_4O_6PPtS_2^+$: 984.1616 $[M + H]^+$; found 984.1660 (3%), *m/z* calcd for $C_{25}H_{24}N_5Pt^+$: 589.1676 $[M - PPh(PhSO_3)_2 + CN]^+$; found 589.1670 (100%). ^1H NMR (500 MHz, D_2O, 65 °C): 8.08 (d, *J* = 4.9 Hz, 4H, bpyH-6/6′), 7.98 (s, 4H, bpyH-3/3′), 7.73 (dd, *J* = 8.4, 2.1 Hz, 4H, H_c), 7.60−7.69 (m, 3H, H_f, H_h), 7.54 (dd, *J* = 11.9, 8.3 Hz, 4H, H_b), 7.47 (td, *J* = 8.1, 2.9 Hz, 2H, H_g), 7.25 (d, *J* = 5.0 Hz, 4H, bpyH-5/5′), 2.47 (s, 12H, CH_3). ^1H NMR (500 MHz, D_2O, 25 °C): 7.85−8.25 (m, broad, 8H, bpyH-6/6′, bpyH-3/3′), 7.61−7.78 (m, 7H, H_c, H_f, H_h), 7.47−7.61 (broad, 4H, H_b), 7.43 (dt, *J* = 7.7, 3.9 Hz, 2H, H_g), 7.05−7.35 (broad, 4H, bpyH-5/5′), 2.45 (s, 12H, CH_3). ^{13}C NMR (126 MHz, D_2O): 158.2 (s, bpyC-2/2′), 157.3 (s, bpyC-4/4′), 152.7−153.8 (broad, bpyC-6/6′), 149.3 (d, ^4J = 2.6 Hz, C_d), 137.1−137.9 (m, broad, C_b, C_f), 136.2 (d, ^4J = 2.8 Hz, C_h), 132.4 (d, ^3J = 11.7 Hz, C_g), 131.0 (s, bpyC-5/5′), 130.4 (d, ^1J = 63.9 Hz, C_a), 129.0 (s, bpyC-3/3′), 128.9 (d, ^3J = 12.1 Hz, C_c), 125.6 (d, ^1J = 63.5 Hz, C_e), 23.5 (s, CH_3). ^{31}P NMR (202 MHz, D_2O): 10.94 (s with satellites; $^1J_{P-Pt}$ = 3795 Hz, $^1J_{P-C}$ = 63.5 Hz and $^2J_{P-C}$ = 11.8 Hz). ^{195}Pt NMR (107 MHz, D_2O): −3197 (d, $^1J_{Pt-P}$ = 3795 Hz).

In Situ Synthesis of $[Pt(bpy)_2(PPh_3)]^{2+}$ in CD_3OD Solution. A pale yellow solution of $[Pt(bpy)_2](NO_3)_2\cdot H_2O$ in CD_3OD (3.0 mM, 1.18 mL) was added to PPh_3 (0.93 mg, 3.5 μmol). The mixture was stirred at room temperature until the PPh_3 dissolved, giving a more intense yellow solution containing $[Pt(bpy)_2(PPh_3)]^{2+}$. HRESI-MS (MeCN): *m/z* calcd for $C_{21}H_{16}N_5Pt^+$: 533.1049 $[M - PPh_3 + CN]^+$; found 533.1039 (100%), *m/z* calcd for $C_{38}H_{31}N_4PPt^{2+}$: 384.5963 $[Pt(bpy)_2(PPh_3)]^{2+}$ $([M]^{2+})$; found 384.5937 (7%). ^1H NMR (500 MHz, CD_3OD): 8.41 (d, *J* = 5.2 Hz, 4H, bpyH-6/6′), 8.33 (d, *J* = 8.0 Hz, 4H, bpyH-3/3′), 8.21 (td, *J* = 7.9, 1.5 Hz, 4H, bpyH-4/4′), 7.50−7.61 (m, 9H, H_b, H_d), 7.48 (ddd, *J* = 7.2, 5.7, 1.1 Hz, 4H, bpyH-5/5′), 7.38−7.44 (m, 6H, H_c). ^{13}C NMR (126 MHz, CD_3OD): 157.1 (s, bpyC-2/2′), 152.9 (s, bpyC-6/6′), 142.6 (s, bpyC-4/4′), 135.7 (d, $^2J_{C-P}$ = 11.2 Hz, C_b), 134.2 (d, $^4J_{C-P}$ = 2.8 Hz, C_d), 130.8 (d, $^3J_{C-P}$ = 11.6 Hz, C_c), 128.9 (s, bpyC-5/5′), 127.0 (s, bpyC-3/3′), 126.1 (d, $^1J_{C-P}$ = 63.7 Hz, C_a). ^{31}P NMR (202 MHz, CD_3OD): 11.91 (s with satellites; $^1J_{P-Pt}$ = 3790 Hz, $^1J_{P-C}$ = 63.6 Hz and $^2J_{P-C}$ = 11.2 Hz).

In Situ Synthesis of $[Pt(4,4'\text{-}Me_2bpy)_2(PPh_3)]^{2+}$ in CD_3OD Solution. A pale yellow solution of $[Pt(4,4'\text{-}Me_2bpy)_2](NO_3)_2\cdot 2H_2O$ in CD_3OD (3.0 mM, 1.41 mL) was added to PPh_3 (1.1 mg, 4.2 μmol). The mixture was stirred at room temperature until the PPh_3 dissolved, giving a more intense yellow solution containing $[Pt(4,4'\text{-}Me_2bpy)_2(PPh_3)]^{2+}$. HRESI-MS (MeCN): *m/z* calcd for $C_{42}H_{39}N_6NaO_6PPt^+$: 972.2212 $[M + 2NO_3 + Na]^+$; found 972.2236 (0.2%), *m/z* calcd for $C_{42}H_{39}N_4PPt^{2+}$: 412.6276 $[Pt(4,4'\text{-}Me_2bpy)_2(PPh_3)]^{2+}$ $([M]^{2+})$; found 412.6230 (2%), *m/z* calcd for $C_{24}H_{24}N_4Pt^{2+}$: 281.5820 $[M - PPh_3]^{2+}$; found 281.5804 (100%). ^1H NMR (400 MHz, CD_3OD): 8.06−8.27 (m, 8H, bpyH-6/6′, bpyH-3/3′), 7.57−7.63 (m, 3H, H_d), 7.52 (dd, *J* = 11.3, 8.2 Hz, 6H, H_b), 7.41 (td, *J* = 7.8, 2.8 Hz, 6H, H_c), 7.27 (d, *J* = 5.7 Hz, 4H, bpyH-5/5′), 2.50 (s, 12H, CH_3). ^{13}C NMR (101 MHz, CD_3OD): δ = 156.8 (s, bpyC-2/2′), 155.6 (s, bpyC-4/4′), 152.0 (s, bpyC-6/6′), 135.7 (d, $^2J_{C-P}$ = 11.2 Hz, C_b), 134.0 (d, $^4J_{C-P}$ = 2.7 Hz, C_d), 130.7 (d, $^3J_{C-P}$ = 11.5 Hz, C_c), 129.4 (s, bpyC-5/5′), 127.6 (s, bpyC-3/3′), 126.4 (d, $^1J_{C-P}$ = 63.6 Hz, C_a), 21.4 (s, CH_3). ^{31}P NMR (202 MHz, CD_3OD): 11.81 (s with satellites; $^1J_{P-Pt}$ = 3801 Hz, $^1J_{P-C}$ = 63.3 Hz and $^2J_{P-C}$ = 11.2 Hz).

Synthesis of $[Pt(bpy)(PPh_3)_2](ClO_4)_2$. PPh_3 (1.06 g, 4.06 mmol) in acetone (40 mL) was added to a stirred suspension of $[Pt(bpy)Cl_2]$ (0.18 g, 0.43 mmol) in H_2O (20 mL). The resulting mixture was stirred at 50 °C for 10 min to give a pale yellow solution. Unreacted PPh_3 precipitated as a white solid upon cooling the mixture on an ice bath. The white solid was removed by filtration, and the pale yellow filtrate was extracted with diethyl ether (3 × 15 mL). $NaClO_4$ (1.88 g) was added to the aqueous layer, and an off-white solid precipitated immediately. The mixture was cooled on an ice bath, the solid was collected by filtration, washed with ice-cold H_2O (4 × 10 mL), then ice-cold EtOH (3 × 10 mL) and finally diethyl ether (3 × 10 mL), and dried under vacuum overnight. Yield: 0.11 g (24%). Anal. Calcd (%) for $C_{46}H_{38}Cl_2N_2O_8P_2Pt$: C 51.41, H 3.56, N 2.61, Cl 6.60; found C 51.34, H 3.50, N 2.70, Cl 6.79. HRESI-MS (MeCN): *m/z* calcd for $C_{28}H_{23}ClN_2O_4PPt^+$: 712.0729 $[M - PPh_3 + ClO_4]^+$ (10%); found 712.0695, *m/z* calcd for $C_{29}H_{23}N_3PPt^+$: 639.1274 $[M - PPh_3 + CN]^+$; found 639.1236 (100%), *m/z* calcd for $C_{46}H_{38}N_2P_2Pt^{2+}$: 437.6075 $[Pt(bpy)(PPh_3)_2]^{2+}$ $([M]^{2+})$; found 437.6050 (1%). ^1H NMR (400 MHz, DMF-d_7): 8.97 (d, *J* = 8.0 Hz, 2H, bpyH-3/3′), 8.52 (t, *J* = 7.8 Hz, 2H, bpyH-4/4′), 8.14−8.22 (broad, 2H, bpyH-6/6′), 8.05−8.14 (m, 12H, H_b), 7.61 (t, *J* = 7.4 Hz, 6H, H_d), 7.50 (t, *J* = 6.8 Hz, 2H, bpyH-5/5′), 7.44 (t, *J* = 7.2 Hz, 12H, H_c). ^{13}C NMR (126 MHz, DMF-d_7): 157.8 (s, bpyC-2/2′), 153.2 (s, bpyC-6/6′), 143.6 (s, bpyC-4/4′), 136.0 (t, $^2J_{C-P}$ = 5.4 Hz, C_b), 133.6 (s, C_d), 130.0 (t, $^3J_{C-P}$ = 5.8 Hz, C_c), 128.5 (s, bpyC-5/5′), 125.8 (d, $^1J_{C-P}$ = 64.6 Hz, C_a), 125.5 (s,

dx.doi.org/10.1021/ic403089j | Inorg. Chem. 2014, 53, 3595−3605

bpyC-3/3′). ^{31}P NMR (162 MHz, DMF-d_7): 8.80 (s with satellites; $^1J_{P-Pt}$ = 3557 Hz). ^{31}P NMR (202 MHz, CD_3OD): 9.15 (broad); no ^{195}Pt satellites were observed owing to the low solubility of the complex in this solvent.

Colorless crystals of $[Pt(bpy)(PPh_3)_2](ClO_4)_2{\cdot}0.5(C_6H_{14}O)$ suitable for X-ray crystallography were obtained by vapor diffusion of diisopropyl ether into a solution of $[Pt(bpy)(PPh_3)_2](ClO_4)_2$ in acetone over 2 d.

X-ray Crystallography. X-ray data were collected at 100.0 K on an Agilent Technologies Supernova system using Mo Kα radiation, and data were treated using CrisAlisPro[40] software. The structure was solved using SIR-97,[41] and weighted full-matrix refinement on F^2 was carried out using SHELXL-97[42] running within the WinGX[43] package.

Data Refinement Details for $[Pt(bpy)_2\{PPh(PhSO_3)_2\}]{\cdot}5.5H_2O$. All non-hydrogen atoms were refined anisotropically. Hydrogen atoms attached to carbons were placed in calculated positions and refined using a riding model. Hydrogen atoms of solvent water molecules were placed in calculated positions and orientated with sensible hydrogen-bonding acceptors (where possible). The two sulfonate groups were disordered over two sites. One group was modeled with occupancies of 40% (O1, O2, and O3) and 60% (O10, O11, and O12) over two sites, and the other group was modeled with occupancies of 50% (O4, O7, and O8) and 50% (O5, O6, and O9) over two sites. S1 and S2 were full occupancy. A DFIX command was used to restrain the S1−O2 distance to 1.35 Å. An ISOR command was applied to sulfonate oxygen atoms O2, O4, O8, O9, and O11 and to the solvent water molecule oxygen atoms O91 and O94. The half of the bpy ring that consists of atoms N4 and C16 through C20 was slightly disordered and modeled with the SIMU command.

Data Refinement Details for $[Pt(bpy)(PPh_3)_2](ClO_4)_2{\cdot}0.5(C_6H_{14}O)$. All non-hydrogen atoms were refined anisotropically. Hydrogen atoms were placed in calculated positions and refined using a riding model. The two isopropyl groups of the diisopropyl ether molecule were slightly disordered. An ISOR command was applied to all six carbon atoms (C91, C92, C93, C94, C95, and C96) in the two isopropyl groups. A DFIX command was used to restrain the O9−C94 distance to 1.44 Å.

Computational Details. All calculations were performed with the Amsterdam Density Functional (ADF 2010)[44−46] package. Functionals based on the generalized gradient approximation (GGA), proposed by Becke[47] and Perdew[48] (for exchange and correlation effects, respectively), and all-electron basis sets of triple-ζ quality plus one polarization function (TZP)[49] were utilized. Relativistic effects were included by means of the zero order regular approximation (ZORA),[50−52] and the conductor-like screening model (COSMO)[53] was used for the treatment of solvation effects, with water as the solvent.

■ ASSOCIATED CONTENT

Supporting Information

Selected ^{1}H, ^{13}C, ^{31}P, and ^{1}H DOSY NMR spectra, selected mass spectra, UV−vis spectra, calculated bonding energy, and CIFs giving crystallographic data for $[Pt(bpy)(PPh_3)_2](ClO_4)_2{\cdot}0.5(C_6H_{14}O)$ (CCDC 975095) and $[Pt(bpy)_2(PPh(PhSO_3)_2)]{\cdot}5.5H_2O$ (CCDC 975096). This material is available free of charge via the Internet at http://pubs.acs.org.

■ AUTHOR INFORMATION

Corresponding Authors

*E-mail: allan.blackman@aut.ac.nz. Fax: +64 9 921 9627. Phone: +64 9 921 9642 (A.G.B.).

*Email: jcrowley@chemistry.otago.ac.nz. Fax: +64 3 479 7906. Phone: +64 3 479 7731 (J.D.C.).

Notes

The authors declare no competing financial interest.

■ ACKNOWLEDGMENTS

The authors are grateful to the National Computational Infrastructure for access to the Australian National University supercomputer facilities. We thank Mr. James Lewis for useful discussions on X-ray crystal structure refinement. W.K.C.L. thanks the University of Otago for awarding a doctoral scholarship.

■ REFERENCES

(1) Gillard, R. D.; Lyons, J. R. *J. Chem. Soc., Chem. Commun.* **1973**, 585−586.

(2) Gillard, R. D. *Inorg. Chim. Acta* **1974**, *11*, L21−L22.

(3) Bielli, E.; Gidney, P. M.; Gillard, R. D.; Heaton, B. T. *J. Chem. Soc., Dalton Trans.* **1974**, 2133−2139.

(4) Gillard, R. D. *Coord. Chem. Rev.* **1975**, *16*, 67−94.

(5) Bielli, E.; Gillard, R. D.; James, D. W. *J. Chem. Soc., Dalton Trans.* **1976**, 1837−1842.

(6) Al-Obaidi, K. H.; Gillard, R. D.; Kane-Maguire, L. A. P.; Williams, P. A. *Transition Met. Chem.* **1977**, *2*, 64−66.

(7) Gameiro, A.; Gillard, R. D.; Bakhsh, M. M. R.; Rees, N. H. *Chem. Commun.* **1996**, 2245.

(8) Nord, G. *Acta Chem. Scand., Ser. A* **1975**, *29*, 270−272.

(9) Farver, O.; Mønsted, O.; Nord, G. *J. Am. Chem. Soc.* **1979**, *101*, 6118−6120.

(10) Constable, E. C. *Polyhedron* **1983**, *2*, 551−572.

(11) Serpone, N.; Ponterini, G.; Jamieson, M. A.; Bolletta, F.; Maestri, M. *Coord. Chem. Rev.* **1983**, *50*, 209−302.

(12) Blackman, A. G. *Adv. Heterocycl. Chem.* **1993**, *58*, 123−170.

(13) McInnes, C. S.; Clare, B. R.; Redmond, W. R.; Clark, C. R.; Blackman, A. G. *Dalton Trans.* **2003**, 2215−2218.

(14) Constable, E. C. *Metals and Ligand Reactivity: An Introduction to the Organic Chemistry of Metal Complexes;* VCH: Weinheim, Germany, 2005; pp 245−250.

(15) Cavigliasso, G.; Stranger, R.; Lo, W. K. C.; Crowley, J. D.; Blackman, A. G. *Polyhedron* **2013**, *64*, 238−246.

(16) Kawanishi, Y.; Funaki, T.; Yatabe, T.; Suzuki, Y.; Miyamoto, S.; Shimoi, Y.; Abe, S. *Inorg. Chem.* **2008**, *47*, 3477−3479.

(17) Wernberg, O.; Hazell, A. *J. Chem. Soc., Dalton Trans.* **1980**, 973−978.

(18) Addison, A. W.; Rao, T. N.; Reedijk, J.; van Rijn, J.; Verschoor, G. C. *J. Chem. Soc., Dalton Trans.* **1984**, 1349−1356.

(19) Note that, in this case, as the τ_5 value involves only the four donor atoms in the square plane, its value is invariant with respect to the positioning of the fifth donor atom. Therefore, any unusual positioning of the axial donor atom will not be reflected in the τ_5 value.

(20) The τ_5 value is calculated from the bond angles reported in reference 17.

(21) Ainscough, E. W.; Brodie, A. M.; Burrell, A. K.; Derwahl, A.; Jameson, G. B.; Taylor, S. K. *Polyhedron* **2004**, *23*, 1159−1168.

(22) Parsons, S.; Brown, A.; Yellowlees, L.; Wood. P. A. Private communication to the CCDC, CCDC 247866, 2004.

(23) Janiak, C. *J. Chem. Soc., Dalton Trans.* **2000**, 3885−3896.

(24) Xue, C.; Métraux, G. S.; Millstone, J. E.; Mirkin, C. A. *J. Am. Chem. Soc.* **2008**, *130*, 8337−8344.

(25) Yang, L.; Powell, D. R.; Houser, R. P. *Dalton Trans.* **2007**, 955−964.

(26) The P atom-to-plane distances are 0.415 and 0.410 Å for P1 and P2, respectively.

(27) Frontera, A.; Gamez, P.; Mascal, M.; Mooibroek, T. J.; Reedijk, J. *Angew. Chem., Int. Ed.* **2011**, *50*, 9564−9583.

(28) A Cambridge structure database (version 5.34 with updates, May 2013) search on Pt−N bond lengths in $[Pt^{II}(bpy)_2]X$ gave the range of Pt−N bond lengths as 2.015−2.044 Å and the average Pt−N bond length as 2.025 Å.

(29) Hazell, A.; Simonsen, O.; Wernberg, O. *Acta Crystallogr.* **1986**, *C42*, 1707−1711.

(30) Fedotova, T. N.; Minacheva, L. K.; Kuznetsova, G. N. *Russ. J. Inorg. Chem.* **2003**, *48*, 351−358.

(31) Clare, B. R.; McInnes, C. S.; Blackman, A. G. *Acta Crystallogr.* **2005**, *E61*, m2042−m2043.
(32) Hudson, T. A.; Robson, R. *Cryst. Growth Des.* **2009**, *9*, 1658−1662.
(33) Stork, J. R.; Rios, D.; Pham, D.; Bicocca, V.; Olmstead, M. M.; Balch, A. L. *Inorg. Chem.* **2005**, *44*, 3466−3472.
(34) Maidich, L.; Zuri, G.; Stoccoro, S.; Cinellu, M. A.; Masia, M.; Zucca, A. *Organometallics* **2013**, *32*, 438−448.
(35) Basolo, F.; Pearson, R. G. *The Mechanisms of Inorganic Reactions: A Study of Metal Complexes in Solution,* 2nd ed.; Wiley: New York, 1967; pp 351−410.
(36) Richens, D. T. *Chem. Rev.* **2005**, *105*, 1961−2002.
(37) Herd, O.; Langhans, K. P.; Stelzer, O.; Weferling, N.; Sheldrick, W. S. *Angew. Chem., Int. Ed. Engl.* **1993**, *32*, 1058−1059.
(38) Morgan, G. T.; Burstall, F. H. *J. Chem. Soc.* **1934**, 965−971.
(39) Livingstone, S. E.; Wheelahan, B. *Aust. J. Chem.* **1964**, *17*, 219−229.
(40) *CrysAlisPro;* Agilent Technologies: Yarnton, Oxfordshire, England, 2012.
(41) Altomare, A.; Burla, M. C.; Camalli, M.; Cascarano, G. L.; Giacovazzo, C.; Guagliardi, A.; Moliterni, A. G. G.; Polidori, G.; Spagna, R. *J. Appl. Crystallogr.* **1999**, *32*, 115−119.
(42) Sheldrick, G. M. *Acta Crystallogr.* **2008**, *A64*, 112−122.
(43) Farrugia, L. J. *J. Appl. Crystallogr.* **1999**, *32*, 837−838.
(44) *Amsterdam Density Functional,* Scientific Computing and Modeling, Theoretical Chemistry; Vrije Universiteit: Amsterdam, The Netherlands (http://www.scm.com).
(45) Guerra, C. F.; Snijders, J. G.; te Velde, G.; Baerends, E. J. *Theor. Chem. Acc.* **1998**, *99*, 391−403.
(46) te Velde, G.; Bickelhaupt, F. M.; van Gisbergen, S. J. A.; Guerra, C. F.; Baerends, E. J.; Snijders, J. G.; Ziegler, T. *J. Comput. Chem.* **2001**, *22*, 931−967.
(47) Becke, A. D. *Phys. Rev. A: At., Mol., Opt. Phys.* **1988**, *38*, 3098−3100.
(48) Perdew, J. P. *Phys. Rev. B* **1986**, *33*, 8822−8824.
(49) van Lenthe, E.; Baerends, E. J. *J. Comput. Chem.* **2003**, *24*, 1142−1156.
(50) van Lenthe, E.; Baerends, E. J.; Snijders, J. G. *J. Chem. Phys.* **1993**, *99*, 4597−4610.
(51) van Lenthe, E.; Baerends, E. J.; Snijders, J. G. *J. Chem. Phys.* **1994**, *101*, 9783−9792.
(52) van Lenthe, E.; Ehlers, A.; Baerends, E. J. *J. Chem. Phys.* **1999**, *110*, 8943−8953.
(53) Pye, C. C.; Ziegler, T. *Theor. Chem. Acc.* **1999**, *101*, 396−408.

dx.doi.org/10.1021/ic403089j | *Inorg. Chem.* 2014, 53, 3595−3605